

The sensitivity of landfast sea ice to atmospheric forcing in single-column model simulations: a case study at Zhongshan Station, Antarctica

Fengguan Gu¹, Qinghua Yang¹, Frank Kauker^{2,3}, Changwei Liu¹, Guanghua Hao⁴,
Chao-Yuan Yang¹, Jiping Liu⁵, Petra Heil⁶, Xuewei Li¹, Bo Han^{1*}

¹ School of Atmospheric Sciences, Sun Yat-sen University, and Southern Marine Science and Engineering
Guangdong Laboratory (Zhuhai), Zhuhai 519082, China

² Alfred Wegener Institute, Helmholtz Centre for Polar and Marine Research, Am Handelshafen 12, 27570
Bremerhaven, Germany

³ Ocean Atmosphere Systems, Tewsstseg 4, 20249 Hamburg, Germany

⁴ Key Laboratory of Marine Hazards Forecasting, National Marine Environmental Forecasting Center, Ministry of
Natural Resources, Beijing 100081, China

⁵ Department of Atmospheric and Environmental Sciences, State University of New York at Albany, Albany, NY,
USA

⁶ Australian Antarctic Division and Australian Antarctic Program Partnership, Private Bag 80, Hobart, Tas 7001,
Australia

Correspondence to: Bo Han (hanb5@mail.sysu.edu.cn)

Abstract

Single-column sea ice models are used to focus on the thermodynamic evolution of the ice. Generally, these models are forced by atmospheric reanalysis in the absence of atmospheric *in situ* observations. Here we assess the sea ice thickness (SIT) simulated by a single-column model (ICEPACK) with *in situ* observations obtained off Zhongshan Station for the austral winter of 2016. In the reanalysis, the surface air temperature is about 1 °C lower, the total precipitation is about 2 mm day⁻¹ larger, and the surface wind speed is about 2 m s⁻¹ higher compared to the *in situ* observations, respectively. We designed sensitivity experiments to evaluate the simulation bias in sea ice thickness due to the uncertainty in the individual atmospheric forcing variables. Our results show that the unrealistic precipitation in the reanalysis leads to a bias of 14.5 cm in sea ice thickness and 17.3 cm in snow depth. In addition, our data show that increasing snow depth works to gradually

inhibit the growth of sea ice associated with thermal blanketing by the snow due to changing the vertical heat flux. Conversely, given suitable conditions, the sea ice thickness may grow suddenly when the snow load gives rise to flooding and leads to snow-ice formation. A potential mechanism to explain the different characteristics of the precipitation bias on snow and sea ice is discussed. The flooding process might cause different effects in landfast sea ice compared to pack ice, but ICEPACK has not distinguished.

1 Introduction

Sea ice plays an essential role in the global climate system by reflecting solar radiation and regulating the heat, moisture, and gas exchanges between the ocean and the atmosphere. In contrast to the rapid decline of sea ice extent and volume in the Arctic (Stroeve et al., 2012; Lindsay and Schweiger, 2015), satellite observations show a slight increase in the yearly-mean area of Antarctic sea ice since the late 1970s (Parkinson and Cavalieri, 2012) followed by a rapid decline from 2014 (Parkinson, 2019) and a renewed increase in most recent years (Chemke and Polvani, 2020). Although the sudden decline of Antarctic sea ice is yet to be attributed (Parkinson, 2019), the spatial pattern of Antarctic sea ice changes is suggested to be primarily caused by changes in the atmospheric forcing. For example, the rapid ice retreat in the Weddell Sea from 2015 to 2017 has been associated with the intensification of northerly wind (Turner et al., 2017), while the phase of the southern annular mode (SAM) significantly modulates the sea ice in the Ross Sea and elsewhere, especially in November 2016 (Stuecker et al., 2017; Schlosser et al., 2018; Wang et al., 2019a).

Landfast sea ice, the immobile fraction of the sea ice, is mainly located in near coastal regions of Antarctica, and its change is assumed to be indicative of the evolution of total Antarctic sea ice (Heil et al., 1996; Heil, 2006; Lei et al., 2010; Yang et al., 2016a). Unlike drifting sea ice, the change in landfast sea ice is dominated by thermodynamic processes, which single-column sea-ice models can well capture (Heil et al., 1996; Lei et al., 2010; Yang et al., 2016b; Zhao et al., 2017). Furthermore, a single-column sea ice model is a useful tool to evaluate the impacts of different atmospheric forcings on the sea ice evolution because of the relatively simple structure of the physical processes (Cheng et al., 2013; Wang et al., 2019b; Merkouriadi et al., 2020). In this study, a state-of-the-art single-column sea ice model, ICEPACK, is chosen to investigate the sensitivity of landfast sea ice to atmospheric forcing for the region off Zhongshan Station in Prydz Bay, East

60 Antarctica (Figure 1).

61 Due to the lack of *in situ* observation, the majority of sea ice studies, especially for the Antarctic,
62 rely on numerical models. Realistic atmospheric forcing is critical for reliable model simulations.
63 Although being criticized for significant deviations from *in situ* observations (Bromwich et al., 2007;
64 Vancoppenolle et al., 2011; Wang et al., 2016; Barthélemy et al., 2018), atmospheric reanalysis data
65 are assumed to offer reasonable atmospheric forcing for large-scale sea ice models for the Antarctic
66 (Zhang, 2007; Massonnet et al., 2011; Zhang, 2014; Barthélemy et al., 2018). Previous studies
67 reported a large spread between four global atmospheric reanalysis products and *in situ* observations
68 in the Amundsen Sea Embayment (Jones et al., 2016). Moreover, studies showed that directly using
69 atmospheric reanalysis as forcing for models causes significant biases in the Arctic sea ice
70 simulations (Lindsay et al., 2014; Wang et al., 2019b). Similar results, accentuated by the sparseness
71 of atmospheric observations entering the reanalysis, can be foreseen for Antarctica. Therefore, the
72 atmospheric forcing needs to be evaluated carefully before simulating Antarctic sea ice. To our
73 knowledge, few studies have given a quantitative evaluation of the effect of different atmospheric
74 forces on sea ice simulations in Antarctica.

75 The coastal landfast sea ice in Prydz Bay is generally first-year ice. It usually fractures and is
76 exported or melts out completely between December and the following February, and refreeze
77 occurs from late February onwards (Lei et al., 2010). This seasonal cycle is representative of
78 Antarctic landfast sea ice. This study aims to evaluate the contributions of the various atmospheric
79 forcing variables on landfast sea ice growth. The snow cover exerts influence on the evolution of
80 the vertical sea ice-snow column via a number of mechanisms, including the formation of snow-ice
81 added by flooding (Leppäranta, 1983), superimposed ice (Kawamura et al., 1997), and insulating
82 impact (Massom et al., 2001). Understanding the snow depth is a primary concern here.

83 Two sets of atmospheric forcing have been chosen. The first is spatially interpolated ERA5 onto
84 the location of the observation site, and the second is using *in situ* atmospheric observations. It is
85 well-known that the simulation biases of numerical models are introduced through many
86 shortcomings, including unrealistic surface boundary conditions (here: atmospheric forcing),
87 imperfect physical process formulations, computational errors. Understanding the uncertainty in sea
88 ice simulations as well as the sea ice response pattern to atmospheric forcing due to imperfect
89 surface boundaries is a prerequisite for successful simulations and needs to be assessed first.

This study is arranged as follows: Section 2 introduces the *in situ* observations, the numerical model, and the reanalysis. The main results are given in section 3, focusing on different kinds of atmospheric forcing on sea ice and snow. Shortcomings, discussions and conclusions follow in sections 4, 5 and 6.

2 Materials and methods

2.1 Meteorological observations

The site of sea ice observation is in the coastal area off Zhongshan Station [(69°22'S,76°22'E); Figure 1], East Antarctica. The meteorological data were collected at a year-round manned weather observatory run at Zhongshan Station in 2016, which is 1 km inland from the sea ice observation site and 15 m above sea level. Snowfall is measured every 12 hours at the Russian Progress II station (located ~1 km to the southeast of Zhongshan Station). The short- and long-wave radiation fluxes were measured every minute with a net radiometer mounted 1.5 m above the surface on a tripod (Yang et al., 2016a). Other meteorological variables are available as hourly data, including 2 m air temperature (T_{2m}), surface pressure (P_a), specific humidity (calculated from dew-point temperature and P_a), potential temperature (calculated from T_{2m} and P_a), air density (calculated by T_{2m} and P_a) and 10 m wind speed (U_{10}) (Hao et al., 2019; Hao et al., 2020; Liu et al., 2020).

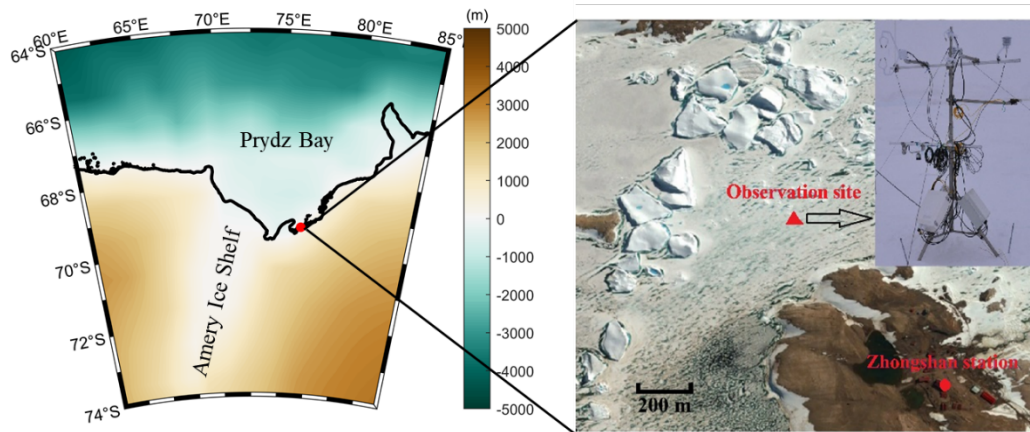


Figure 1 Location of landfast sea ice surface measurements near Zhongshan Station. The solid triangle denotes the observation site, the solid circle marks Zhongshan Station. The color on the left represents the terrain.

2.2 Sea ice thickness measurement

A thermistor-chain unit developed by Taiyuan University of Technology (TY) was used to measure sea ice thickness in austral winter 2016. This unit is composed of two parts: the control unit and the thermistor chain. The controller initiates data acquisitions and records and stores the temperature measurements. The thermistor chain is 3 m long with 250 equidistant thermistors. Their sensitivity is 0.063 °C, and the measurement accuracy is better than ± 0.5 °C. The thermistor chain simultaneously records the vertical temperature profile across the near-surface atmosphere, snow cover, sea ice, and surface seawater. The measurement frequency is hourly. Details about the instruments can be found in Hao et al. (2019).

Snow thickness close to the thermistor unit is measured weekly using a ruler with an accuracy of ± 0.2 cm. Sea ice thickness is measured with a ruler through a drill hole (5 cm diameter) weekly. The measurement accuracy is ± 0.5 cm. The average thickness obtained from three close-by sites is retained. Sea-surface temperature and sea-surface salinity are measured in the drill holes weekly using a Cond 3210 set 1 (Hao et al., 2019).

2.3 Atmospheric reanalysis data

The European Centre for Medium-range Weather Forecasts (ECMWF) released ERA5, the new reanalysis product in 2017, updated in near real-time (Hersbach and Dee, 2016; Hersbach et al., 2020). The complete ERA5 dataset, extending back to 1950, has been available to the end of 2019 during this study. Compared with the popular ERA-Interim reanalysis, there are several significant improvements in ERA5, including much higher resolutions (both spatially and temporally). ERA5 has global coverage with a horizontal resolution of 31 km by 31 km at the equator and 10 km by 31 km at the latitude of Zhongshan Station. The ERA5 resolves the vertical atmosphere profile using 137 vertical pressure levels from the surface up to a geopotential height of 0.01 hPa. ERA5 provides hourly analysis and forecast fields and applies a four-dimensional variational data assimilation system (4D-var). ERA5 includes various reprocessed quality-controlled data sets, for example, the reprocessed version of the Ocean and Sea Ice Satellite Application Facilities (OSI SAF) sea ice concentration (Hersbach and Dee, 2016; Hersbach et al., 2020).

For comparison and evaluation against the observation in this study, gridded data from ERA5 has been bilinearly interpolated to the observation site (detailed in 2.1). Directly using atmospheric

forcing from coarse grid cells to interpolate to the observation site, although widely accepted in the previous studies (e.g., Urraca et al., 2018; Wang et al., 2019b), may cause errors. We have checked the performance of ERA5 and found that the spatial difference of surface atmospheric variables around the observation site is relatively small, indicating the choice of interpolation techniques will not affect the conclusion of this study.

2.4 ICEPACK

ICEPACK is a column-physics component of the Los Alamos Sea Ice Model (CICE) V6 and is maintained by the CICE Consortium. ICEPACK incorporates column-based physical processes that affect the area and thickness of sea ice. It includes several options for simulating sea ice thermodynamics, mechanical redistribution (ridging), and associated area and thickness changes. In addition, the model supports several tracers, including ice thickness, enthalpy, ice age, first-year ice area, deformed ice area and volume, melt ponds, and biogeochemistry (Hunke et al., 2019). ICEPACK Version 1.1.1 was used in this study, and detailed options of physical parameterizations and model settings for the ICEPACK are summarized in Table 1. We employ ICEPACK to distribute the initial ice thickness to each ice thickness category using a distribution function:

$$p_i = \frac{\max(2 \times h \times H_i - H_i^2, 0)}{\sum_i \max(2 \times h \times H_i - H_i^2, 0)}, \quad i = 1 \dots N, \quad (1)$$

Where h is the initial ice thickness, H_i is the prescribed ice thickness category (0–0.6, 0.6–1.4, 1.4–2.4, 2.4–3.6, and above 3.6 m~; same as for Arctic simulations), N is the number of ice thickness categories.

Table 1 Detailed options of physical parameterizations and model settings for the ICEPACK.

ICEPACK	Value
time step	3600 s
Number of layers in the ice	7
Number of layers in the snow	1
Ice thickness categories	5 (Bitz et al., 2001)
Initial ice thickness	99.5 cm (observed)
Initial snow depth	11.5 cm (observed)
Albedo scheme	CCSM3 (Collins et al., 2006)
Ice thermodynamic	Mushy-layer (Turner et al., 2013)
Shortwave radiation	Delta-Eddington (Briegleb and Light, 2007)
Snowdrift	Not implemented in ICEPACK 1.1.1
Melt ponds (superimposed ice)	Not used in this study

The atmospheric forcing for the ICEPACK model consists of observations of downward short- and long-wave radiation, 2 m air temperature, specific humidity, total precipitation, potential temperature, 2 m air density, and 10 m wind speed. The oceanic forcing includes sea surface temperature, sea surface salinity, and oceanic mixed layer depth. The period concerned in this study is from April 22, when observed sea ice generally starts to grow, to November 22 in 2016. Since there are no observations of the ocean's mixed-layer depth, we set it to 10 m based on a previously published study (Zhao et al., 2019).

3 Results

3.1 Surface atmospheric conditions near the observation site

First, we compare the eight atmospheric variables used to force ICEPACK (surface downward shortwave radiation (R_{sd}), surface downward long-wave radiation (R_{ld}), surface air temperature (T_a), specific humidity (Q_a), precipitation (P), air potential temperature (θ_a), air density (ρ_a), wind speed (U_a) with the respective *in situ* observation. Table 2 lists the bias (simulation minus observation), bias ratio (ratio between the bias and the observation value), the mean value of the *in situ* observation (Mean_Obs), the correlation coefficient (Corr.), and the root-mean-square deviation (RMSD) between the interpolated ERA5 data and the observation. In general, all eight variables from the two sources closely follow each other (Corr. > 0.85), except for P and U_a . In this study, the main attention is on the atmospheric variables T_a , P , and U_a for three reasons: (1) Previous studies have shown that from all atmospheric forcing variables, uncertainties in T_a , P , and U_a exert a significant impact on the sea ice thickness (Cheng et al., 2008). (2) Surface wind may affect the snow cover in two ways: sublimation due to surface turbulent heat flux (Fairall et al., 2003; Gascoin et al., 2013) and snowdrift process (Thiery et al., 2012). (3) P and U_a from the reanalysis have the largest bias ratio compared to the *in situ* observations.

The timing of daily variations of T_a is well represented by ERA5, especially for strong cooling events (Figure 2a). However, ERA5 tends to underestimate warm events by a few degrees as well as cold events where differences exceeding 10 °C may occur (Figure 2d). During the entire observation period in 2016, T_a from ERA5 was 1.168 °C lower than the *in situ* observation. Also, previous studies reported similar disagreement in T_a between observation and reanalysis in Antarctica (Bracegirdle and Marshall, 2012; Fréville et al., 2014). The cold bias of T_a in the

reanalysis was suggested to be caused by the ice surface schemes that cannot accurately describe the ice-atmosphere interactions of strongly stable stratified boundary layers that are frequent in Antarctica.

Table 2 Comparison of atmospheric forcing between ERA5 reanalysis and *in situ* observations.

Variable	Bias	Bias ratio (%)	Mean_Obs	Corr	RMSD
R_{sd} (W m ⁻²)	6.115	9.031	67.714	0.967	40.981
R_{ld} (W m ⁻²)	-19.153	-9.672	198.023	0.869	28.753
T_a (K)	-1.168	-0.453	257.809	0.967	2.820
Q_a (10 ⁻⁴ kg kg ⁻¹)	-0.769	-9.326	8.247	0.950	1.987
P (mm day ⁻¹)	2.010	303.509	0.660	0.639	0.825
Θ_a (K)	0.290	0.112	259.437	0.965	2.609
ρ_a (kg m ⁻³)	-0.021	-1.592	1.322	0.958	0.026
U_a (m s ⁻¹)	2.145	50.735	4.228	0.765	2.989

The reanalyzed variable with the largest bias ratio from the observation is the precipitation (Figure 2b). Hourly precipitation from ERA5 was accumulated into daily data and compared with the nearest available daily precipitation records from the Progress II station. The maximum daily mean precipitation can reach 19.1 mm day⁻¹ (July 11, 2016) with an average of 0.66 mm day⁻¹ from April 29 to November 22, 2016. While ERA5 captures the main precipitation events, it significantly overestimated the magnitude of precipitation events, especially in July. In this month, the mean precipitation rate from ERA5 is 5.83 mm day⁻¹, while the observed is only 1.42 mm day⁻¹. From April to November, the accumulated precipitation from ERA5 is about 300% larger than that in the *in situ* observations. Nevertheless, using precipitation from Progress II for Zhongshan Station may be questioned because of the distance of about 1 km to Zhongshan Station. Moreover, the snowdrift due to strong surface wind can affect the precipitation observation and the local accumulated snow mass, which may further cause a significant bias in snow depth between simulation and observation.

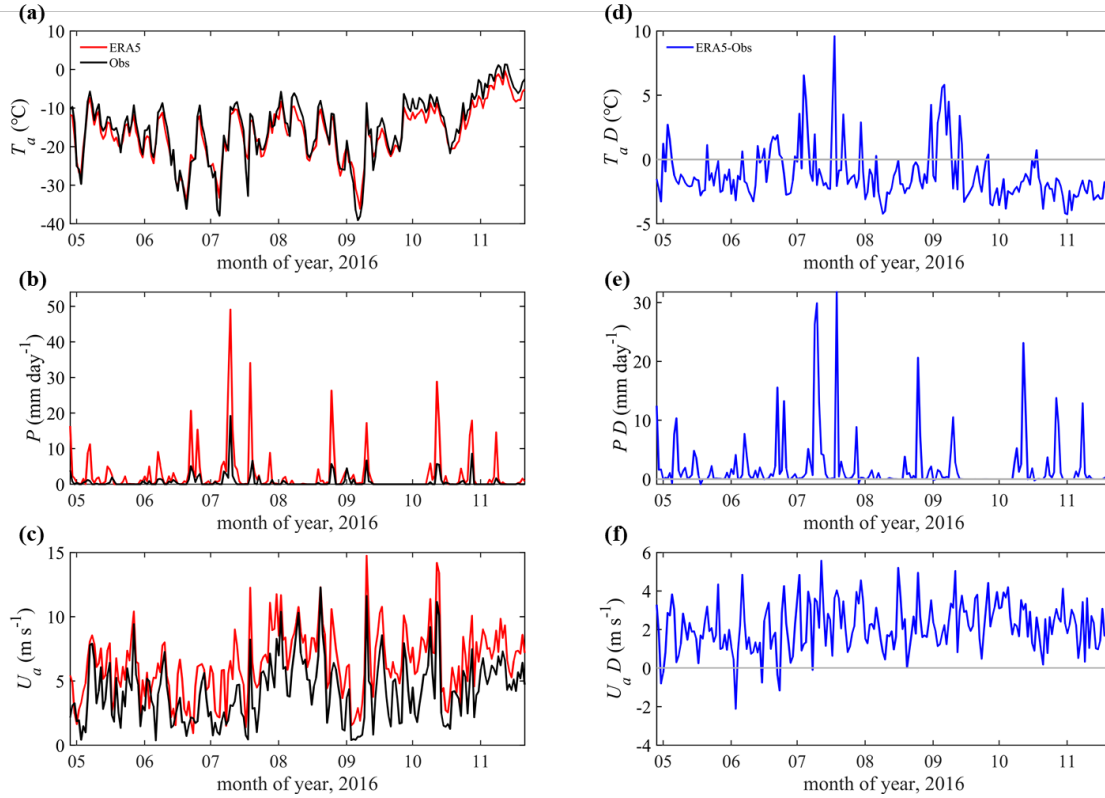


Figure 2 Time series of daily (a) surface air temperature, (b) precipitation rate, and (c) wind speed (10 m above the surface). The ERA5 reanalysis data are indicated as red lines. Observations are marked by black lines. (d-f) show the difference (marked by 'D') between ERA5 and the observation (ERA5-observation). The differences are marked by blue lines. The gray lines denote the zero line.

The observed U_a varied from 0.01 m s^{-1} to 12.3 m s^{-1} with an average of 4.2 m s^{-1} (Figure 2c). ERA5 well captured the daily and seasonal variation of U_a , but an overestimation of 2.1 m s^{-1} should be noted, mainly when observed $U_a > 5 \text{ m s}^{-1}$. One explanation for such overestimation is that the numerical model underlying ERA5 cannot represent the surface roughness and the katabatic wind in a region with complex orography (Tetzner et al., 2019; Vignon et al., 2019).

3.2 Simulation forced by observed *in situ* atmospheric variables

The simulation bias of sea ice thickness and snow depth is impacted by many aspects, including unrealistic atmospheric and oceanic forcing and shortcomings in the applied numerical model. In this study, we mainly focus on the influence of imperfect atmospheric forcing.

The sea ice thickness (Obs) measured through a hole drilled is increasing from April 29 (100 ± 2

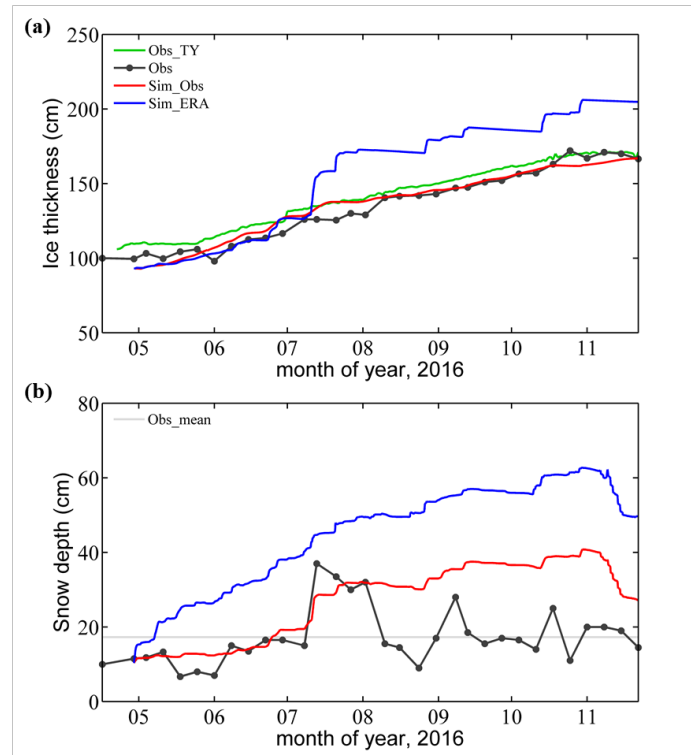
cm) to October 25 (172 ± 2 cm), remaining level from there on (Figure 3a). The ice thickness deduced from the TY (Obs_TY) thermistor-chain buoy shows a similar result: sea ice thickness increased from 106 cm on April 22 to 171 cm on November 17. In November, the sea ice thickness (Obs and Obs_TY) is stationary, indicating a thermodynamic equilibrium between heat loss to the atmosphere and heat gain from the ocean (Yang et al., 2016a; Hao et al., 2019).

When forced by atmospheric *in situ* observations (Sim_Obs), the simulated sea ice thickness agrees well with the observed thickness with a mean bias of less than 1 cm over the growing season. We attribute the excellent simulation result to the fact that the seasonal evolution of landfast is driven mainly by thermal processes, which ICEPACK captures well.

The average snow depth from observation is 17 cm during the ice-growth season, with low snow depth measured before July 11 (Figure 3b). After that, the snow depth increases rapidly up to about 37 cm associated with a precipitation event arising from a single synoptic system. Then it decreases below the seasonal mean (Obs_mean) followed by two secondary maxima (> 25 cm) on September 8 and October 18, respectively.

The snow depth in Sim_Obs tracks the observation closely before August 2 (Figure 3b). Then, the Observed snow depth decreased quickly from about 30 cm to about 10 cm, while the Sim_Obs snow depth continued to increase gradually until the onset of surface melting in November. We attribute the Observed quick decrease of snow depth to the effect of the snowdrift because the surface wind stayed above 5 m s^{-1} for most of August (Figure 2c), giving rise to snowdrift, a process not implemented in the version of ICEPACK used here. The snowdrift might cause a significant spatial difference in accumulated snow patterns (Liston et al., 2018), which may be responsible for the large deviation in snow depth between Sim_Obs and Observation. In addition, Sim_Obs underestimated the snow depth on July 11. As discussed above, using nonlocal observed precipitation from Progress II should be questioned.

Using observed meteorological variables as atmospheric forcing in ICEPACK produced unreliable snow depth while the sea ice thickness was in reasonably good agreement. In other words, the enormous bias in snow depth seems to have little effect on the sea ice thickness in the simulation. This counter-intuitive finding is of great interest to us because it disobeys the general realization that the snow layer significantly modifies the energy exchange on top of the sea ice. Potential causes for this result will be discussed later.



262

263 Figure 3 Time series of (a) sea ice thickness and (b) snow depth during the freezing season. Black
 264 solid lines with black points show the observations from the drill hole (Obs). Green solid lines show
 265 the ice thickness derived from the TY buoy (Obs_TY). Red solid lines show the simulation results
 266 under *in situ* atmospheric forcing (Sim_Obs), and blue solid lines are simulation results under ERA5
 267 forcing (Sim_ERA). In (b), the gray solid line shows the seasonal mean snow depth observation
 268 (Obs_mean).

269

270 3.3 Simulation forced by ERA5 atmospheric variables

271 When forced by ERA5 (Sim_ERA), the simulated sea ice thickness shows significant deviations
 272 from observation (Figure 3a). The deviation is only about 1 cm before July 11, when a heavy
 273 precipitation event ($\sim 19 \text{ mm day}^{-1}$) happened. After the precipitation episode, the offset in the sea
 274 ice thickness between Sim_ERA and observation was almost constant, about 33 cm.

275 In contrast to sea ice thickness, the precipitation from ERA5 causes an overestimation in snow
 276 depth for the entire simulation period. The snow depth from Sim_ERA is much greater than
 277 observation, even before July 11 (Figure 3b). During the heavy precipitation event (Figure 2b), the
 278 observed snow depth increased from 20 cm to about 40 cm. Although the precipitation rate from

ERA5 ($\sim 40 \text{ mm day}^{-1}$) is two times larger than the observation, it caused little response in the simulated snow depth. The snow depth increase is near-linear, from about 10 cm to almost 60 cm.

3.4 Sensitivity analysis

The results from Sim_ERA are connected with the sensitivity of sea ice and snow depth to atmospheric forcing change. To determine the sensitivity of sea ice and snow depth near Zhongshan station on atmospheric forcing, we designed a set of numerical experiments named SEN1. In the control run, the forcing of the simulation directly used the means of observed atmospheric variables (Mean_Obs in Table 3). For a specific atmospheric variable, we build a set of sensitive runs. The focused atmospheric variable changed from its mean (Range in Table 3), and other variables are the same as the control run. Considering the actual range in each observed variable, we set the maximum change in T_a , Θ_a , and ρ_a to 2%, and other atmospheric variables to 50%. Then, we concluded the sensitivity of sea ice and snow to each atmospheric forcing from its corresponding sensitive runs. Because sea ice and snow depth show a quasi-linear response to the change in each specific atmospheric forcing (not shown), the choice of the variable's range will not alter the sensitivity results.

Table 3 The atmospheric forcing (Mean_obs for the control run and range for the sensitive run), sensitivity, and potential bias from SEN1.

Variable	Mean_Obs (Control)	Range (%)	Sensitivity		Potential Bias	
			Ice (cm/%)	Snow (cm/%)	Ice (cm)	Snow (cm)
$R_{sd} \text{ (W m}^{-2}\text{)}$	67.714	± 50	-0.033	-0.008	-0.295	-0.069
$R_{ld} \text{ (W m}^{-2}\text{)}$	198.023	± 50	-0.368	-0.201	3.559	1.944
$T_a \text{ (K)}$	257.809	± 2	-1.247	-0.526	0.565	0.238
$Q_a \text{ (10}^{-4} \text{ kg kg}^{-1}\text{)}$	8.247	± 50	-0.025	0.029	0.230	-0.270
$P \text{ (mm day}^{-1}\text{)}$	0.660	± 50	-0.032	0.135	-9.712	40.974
$\Theta_a \text{ (K)}$	259.437	± 2	-1.297	-0.491	-0.145	-0.055
$\rho_a \text{ (kg m}^{-3}\text{)}$	1.322	± 2	-0.054	0.021	0.086	-0.033
$U_a \text{ (m s}^{-1}\text{)}$	4.228	± 50	-0.054	-0.022	-2.748	-1.116

In Table 3, the sensitivity of ice thickness and snow depth to each atmospheric variable are listed. Comparing the individual sensitivity, it turns out that the sea ice thickness and snow depth are most

sensitive to T_a and Θ_a . However, since T_a and Θ_a from ERA5 is close to the *in situ* observation, the potential bias contributed by these two terms is relatively small. In contrast, the most significant overestimation in P in ERA5 is the primary source for the simulation bias for sea ice thickness and snow depth.

To clarify the effect of specific forcing further, we replaced the x forcing in Sim_Obs with the corresponding ERA5 variable and named it Sim_ERA_x. Compared with Sim_Obs, Sim_ERA_P overestimates the snow depth since May (Figure 4b) and shows a significant positive bias in sea ice thickness after July 11 (Figure 4a). Before July 11, the sea ice thickness from Sim_ERA_P was even smaller than that from Sim_Obs.

To find out why the snow and sea ice behaves differently, we first investigate the net heat flux into the ice surface H_N (positive downward):

$$H_N = Rn + Hs + Hl, (2)$$

where Rn , Hs , and Hl are the net surface radiation flux, the sensible heat flux, and the latent heat flux, respectively. All energy fluxes are defined as positive downward. Because the simulated snow layer in SIM_ERA_P is much deeper than in SIM_Obs, the difference of H_N reflects the modification of the surface energy flux due to the changed snow layer. From Figure 4d, it can be deduced that the overestimation of snow depth in SIM_ERA_P results in a positive anomaly of H_N before July 11, which hampers the sea ice growth. Later the difference of H_N becomes relatively small. The dependence of H_N on the snow depth is significant when the snow layer is shallow (<20 cm in this study). If the snow layer is deep enough, its impact on the net surface heat flux ceases.

After July 11, the difference in sea ice thickness between the two simulations increases quickly from ~0 to >40 cm (Figure 4a). We attribute that to flooding with subsequent snow-ice formation (Powell and others, 2005). The continuously deepening snow layer reduces the sea ice freeboard. When heavy snowfall occurs, which frequently happens after July 11, the snow load pushes the sea ice surface below sea level, and seawater floods onto the sea ice surface, causing the overlying snow to freeze. This snow-ice formation process will form flooding ice (snow-ice thickness) at the sea ice surface and rapidly increase the total sea ice thickness (Figure 4a). The difference (~100 cm) in accumulated flooding ice (Figure 4c) between Sim_Obs (0.8 cm) and Sim_ERA_P (105.5 cm) is much greater than the difference (~40 cm) in simulated sea ice thickness (Figure 4a), while the net surface heat flux compares well after July 11 (Figure 4d). This difference may be because as the

snow-ice process occurs, the increase in sea ice thickness will reduce the heat transfer between the ocean and the atmosphere and inhibit the basal growth of sea ice in winter (Figure 4e). The flooding-induced snow-ice formation happens with a rate larger than 0.5 cm per hour after July 11. The snowfall (Figure 2b) is converted to new snow depth at the top surface (Figure 4f) using a snow density of 330 kg m^{-3} in ICEPACK (Hunke et al., 2019). Comparing Figure 4b with Figure 4f, we find that the change in actual snow depth (11 cm) is much lower than the expected accumulated snowfall (57 cm), indicating the flooding process reduces about four-fifths of snow depth over sea ice.

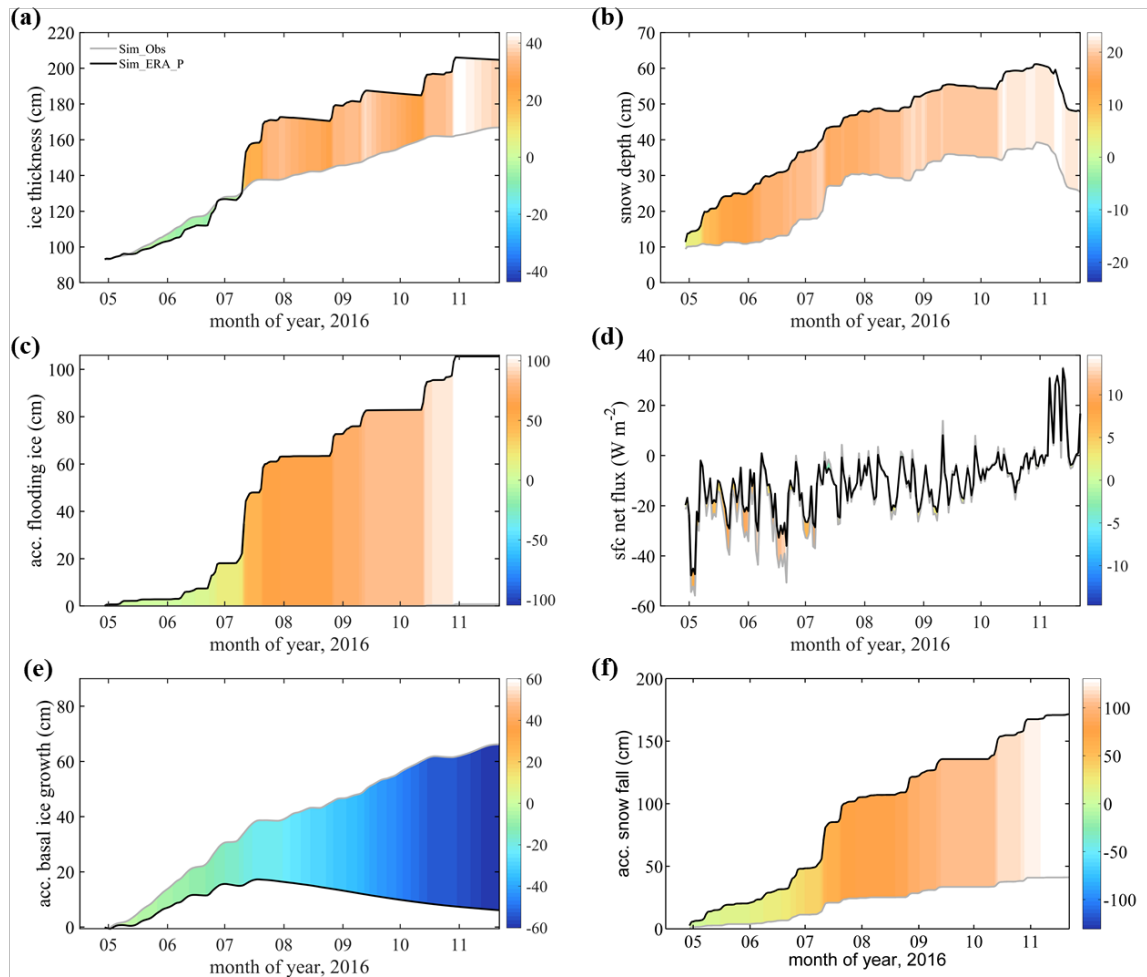


Figure 4 Times series of (a) sea ice thickness, (b) snow depth, (c) accumulated flooding ice, (d) net surface heat flux, (e) accumulated basal ice growth, and (f) accumulated snowfall. The gray line represents the simulation using precipitation from observation (Sim_Obs). The black line represents the simulation using precipitation from ERA5 (Sim_ERA_P). The color bar represents their difference (Sim_ERA_P – Sim_Obs).

3.5 Additional sensitivity simulations on the precipitation bias

The precipitation from ERA5 shows the most significant deviation compared to the *in situ* observation and contributes the largest to the sea ice and snow simulation bias. To determine the cause of differences in the sea ice and snow response to precipitation, we set up ten sensitivity experiments named SEN2 (Figure 6). In the n -th experiment, $n \times 10\%$ of the daily difference between P from ERA5 and the *in situ* observation is added to the observed P on that day. This procedure gradually increases the magnitude of the precipitation in the experiments, while the timing of the daily precipitation events remains almost unchanged.

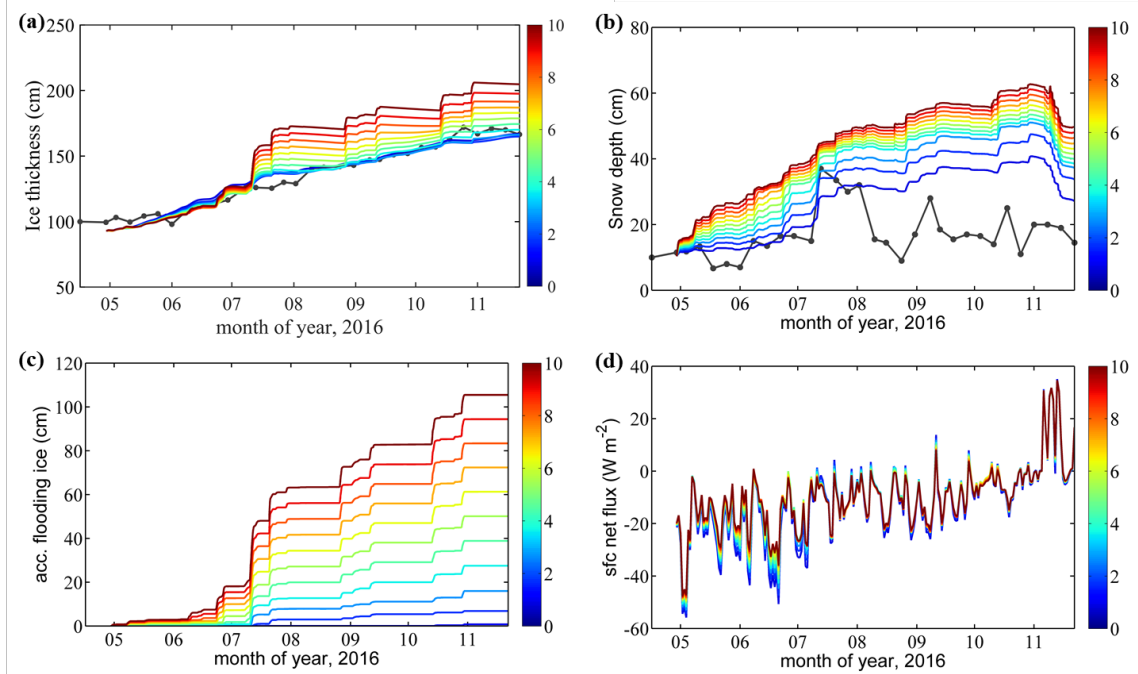


Figure 6 Time series of the simulated (a) sea ice thickness, (b) snow depth, (c) accumulated flooding ice, and (d) net surface heat flux in the n experiments of SEN2. The black solid point lines show the *in situ* observations (Obs). The 11 colored lines denote the 11 sensitivity experiments. When $n = 0$, precipitation is from the *in situ* observation. When $n = 10$, precipitation is from ERA5.

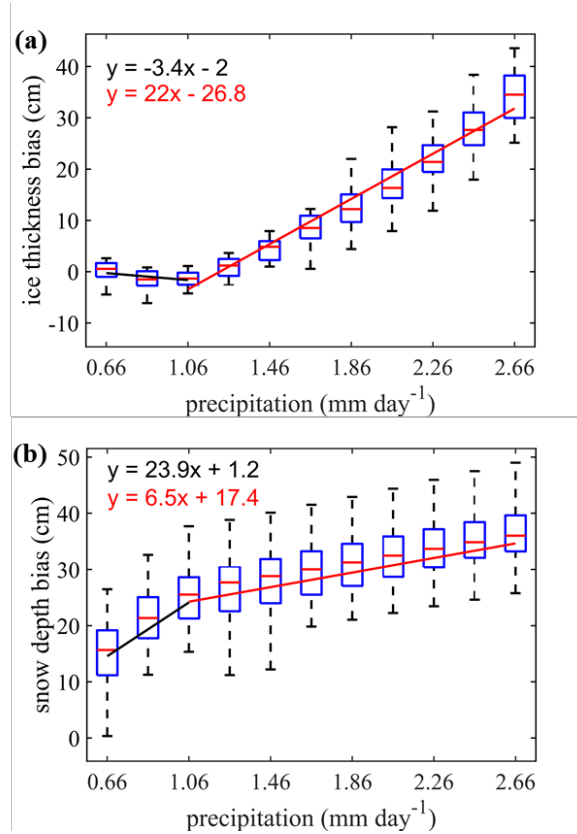


Figure 7 Box plot of simulation bias (simulation minus observation) of (a) sea ice thickness and (b) snow depth over the daily mean precipitation in the different sensitivity experiments (n increases from left to right). On the x-axis, 0.66 mm refers to the experiment with $n=0$ (*in situ* precipitation), and 2.66 mm refers to the $n=10$ experiment (ERA5 precipitation). Two linear regression lines (black and red) are derived for $x \leq 1.06$ mm and $x > 1.06$ mm based on the mean of ice thickness and snow depth.

We define the bias as the difference between simulations and observations from July 27 to the end of November. Different start or end dates of this period do not change this result. The bias of both sea ice thickness and snow depth linearly grows with increasing precipitation (Figure 7). The simulation bias of the sea ice thickness is relatively small before the precipitation increases by about 1 mm per day. We suggested that the snow-ice formation is small (Figure 6c), and the insulation of the snow layer (Figure 6d) hampers the sea ice growth. In fact, the simulated sea ice thickness even decreases (at a rate of $-3.4 \text{ cm}/(\text{mm day}^{-1})$) when the added precipitation is $< 1 \text{ mm day}^{-1}$. When the added precipitation is $> 1 \text{ mm day}^{-1}$, the simulated sea ice thickness quickly increases at a rate of $22 \text{ cm}/(\text{mm day}^{-1})$.

In contrast, the simulated snow depth deepens rapidly at $23.9 \text{ cm}/(\text{mm day}^{-1})$ when the enforced

precipitation remains small but at a rate of 6.5 cm when the added precipitation is large. This is because more snow is converted into flooding ice, and the snow-ice formation process strongly overrules the larger insulation effect from the snow layer, promoting sea ice growth.

The snow-ice process is based on Archimedes' Principle. Therefore, the threshold value (1 mm/day⁻¹) is related to the density value of ice, snow, and water in model parameterization as well as the sea ice thickness and snow depth. If sea ice and snow density, initial snow depth decrease, or seawater density and initial ice thickness increase, the threshold will increase, and vice versa. These different effects of increases in precipitation on the snow and sea ice growth are illustrated in Figure 8, emphasizing the role of flooding via snow-ice formation. When the snow layer is shallow, increases in precipitation will quickly deepen the snow layer and inhibit the growth of sea ice thickness due to the insulation of snow. The decrease in the surface net heat flux is the dominant factor. While the snow layer is deep and large precipitation is present, the flooding process induces snow-ice formation, and the sea ice grows quickly while the snow depth increases only slowly.

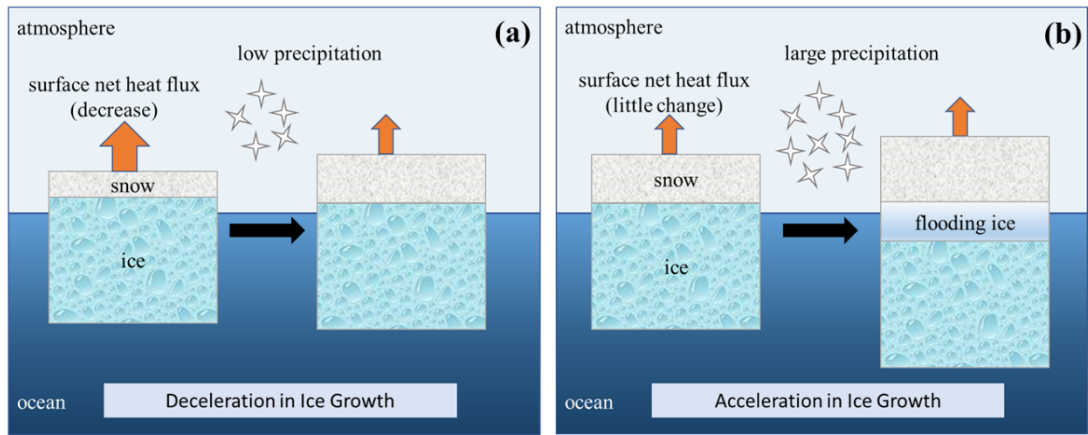


Figure 8 Schematic diagram for (a) low precipitation and (b) large precipitation events illustrating the precipitation effect on sea ice growth. The orange arrows represent surface net heat flux, and different colored boxes indicate the layer of snow, flooding ice, and sea ice.

4 Shortcomings

Superimposed ice is present in early autumn when the snow starts to melt (Kawamura et al., 1997) and contributes significantly to sea ice growth (up to 20% of mass) (Granskog et al., 2004). Superimposed ice usually corresponds to liquid precipitation or melted snow that permeates downward to form a fresh slush layer and refreezes. The superimposed ice is implemented in

ICEPACK via the melt ponds parametrization but has not been considered in this study because the deformation information of sea ice is not available. Therefore, the simulation may underestimate sea ice thickness and overestimate snow depth compared to observation in November. We will apply the melt ponds scheme in the follow-up research work.

The snow-ice formation might be overestimated on the landfast sea ice in ICEPACK. Flooding-induced snow-ice formation is common in the Antarctic ocean because of the thin ice and heavy snowfall (Kawamura et al., 1997). It can contribute to considerable ice mass (12%-36%) and reduce the snow depth by up to 42-70%, depending on the season and location (Jeffries et al., 2001). The parameterization of the flooding process in the ICEPACK is based on Archimedes' Principle for the pack ice, which might be problematic for the coastal landfast sea ice. With a much larger volume and shallower seawater around than the pack sea ice, part of the coastal landfast sea ice might contact the sea bed rather than float in the sea. Thus, the flooding should be much weaker even with weighted snow cover. Besides, the change in density of ice due to the flooding process is significant (Saloranta, 2000) but not well considered in ICEPACK. For example, a slushy layer of 10 cm depth would refreeze within three days from observation (Provost et al., 2017), while the process only needs one day in ICEPACK. Hence, the landfast sea ice growth due to snow-ice formation needs improvement in ICEPACK, especially when the input precipitation is significantly exaggerated, e.g., the ERA5 forcing.

5 Discussions

Surface drifting snow particles play an essential role in the surface mass balance (Van den Broeke et al., 2004). Figure 3b shows that the observed snow depth has quickly decreased from 32 cm on August 2 to 15.5cm on August 10, which should be attributed to the snowdrift because the surface wind is $> 8 \text{ m s}^{-1}$ in most of this period (Figure 2c). Friction velocity becomes sufficiently high to overcome the gravity and bonds between snow particles in this strong wind and raise the snow particles from the surface (van den Broeke et al., 2006; Thierry et al., 2012; Tanji et al., 2021). However, the mean surface wind in ERA5 is convergent around the observation site during the intense wind period (Figure 8), which might not be expected for snow depth decrease due to snowdrift. The coarse resolution of the atmospheric reanalysis might not produce a realistic surface wind field, which is primarily determined by the topography (Van Den Broeke et al., 1999; Frezzotti

et al., 2005). In addition, surface sublimation of drifting snow particles, which is most significant in warm, dry, and windy weather (Thiery et al., 2012), plays an important role in surface mass balance (Van den Broeke et al., 2004) but has not been involved in ICEPACK yet.

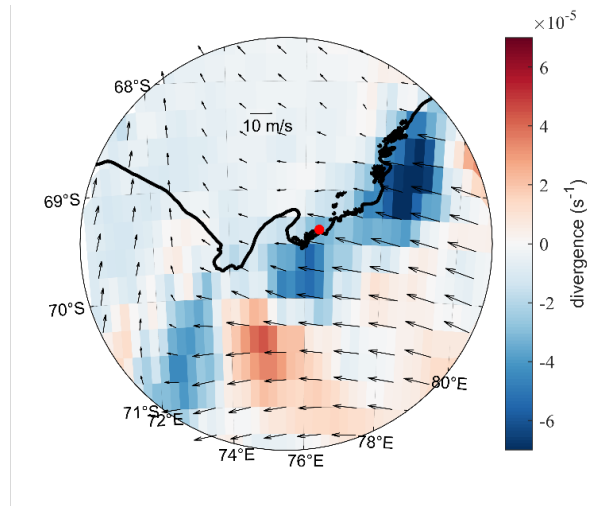


Figure 8 The mean ERA5 surface wind and divergence from August 2 to 10. The black line represents the coastline, and the red point represents the observation site.

The surface wind can affect the snow depth by changing the surface heat fluxes (Fairall et al., 2003). Compared with Sim_Obs, Sim_ERA_W gives a $-2.5 \times 10^4 \text{ W m}^{-2}$ lower latent heat flux (positive downward) on average (Figure 9b), i.e., a larger sublimation (Figure 9c), and a reduction of about -3.4 cm of the snow depth (Figure 9a). Therefore, the overestimation in the surface wind from ERA5 partly neutralizes the effect of overestimated precipitation.

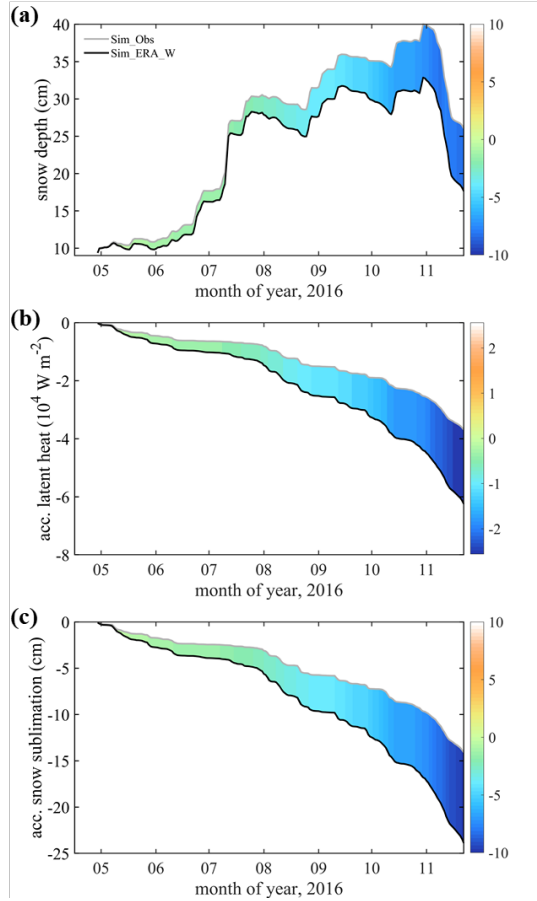


Figure 9 Times series of (a) snow depth, (b) accumulated latent heat flux, and (c) accumulated snow sublimation. The gray line represents the simulation using wind from the observation (Sim_Obs). The black line represents the simulation using wind from ERA5 (Sim_ERA_W). The color bar represents their difference (Sim_ERA_W – Sim_Obs).

The oceanic forcing also plays an essential role in sea ice evolution (Uotila et al., 2019). Heat flux from the ocean boundary layer changes the sea ice energy balance (Maykut and Untersteiner, 1971). The ocean heat flux is mainly impacted by summer insolation through open leads, thin ice, melt ponds (Perovich and Maykut, 1990), and upward heat transfer through vertical turbulent mixing (McPhee et al., 1999). Because the oceanic observations under sea ice are challenging, most sea ice models directly use some empirical values, like the default value in CCSM3, to build the ocean boundary condition (e.g., Yang et al., 2016b; Turner and Hunke, 2015). In this study, although some oceanic variables, like the water temperature and salinity, are from observation, while others, like the mixed layer depth, simply refers to previous studies. The uncertainty in oceanic forcing might be as important as the atmospheric ones, which will be focused in our coming work.

6 Conclusions

This work uses the single-column sea ice model ICEPACK forced by the ERA5 atmospheric reanalysis and atmospheric *in situ* observations to simulate snow depth and sea ice thickness at Zhongshan Station, Antarctic. The main results are listed below:

- (1) Forcing by atmospheric variables from *in situ* observations, the ICEPACK can well simulate the sea ice evolution but significantly overestimates the snow depth. When using atmospheric forcing from ERA5, sea ice thickness simulation is close to observation before July 11, but then suddenly increases in an extremely large precipitation event. For the entire simulation period, ERA5 obviously causes an overestimation in snow depth compared to observation.
- (2) Although sea ice sensitivity ($-0.032 \text{ cm}/\%$) is small and snow thickness sensitivity ($0.135 \text{ cm}/\%$) is moderate to precipitation in ICEPACK, the significant deviation in the reanalysis's precipitation contribute to the largest bias in both sea ice thickness and snow depth. On average, about 2 mm day^{-1} more precipitation in ERA5 is found during the observation period, which produces about 14.5 cm excess in sea ice thickness and 17.3 cm more snow depth.
- (3) The flooding process can be triggered by a heavy snowfall episode, like on July 11. It efficiently produces ice at the sea ice surface, decelerates the snow accumulation, and inhibits sea ice's basal growth.
- (4) The interaction between sea ice and its covering snow determines their response to snowfall. When the snowfall is weak, the snow layer thickens quickly and hampers the sea ice growth through its insulation effect. When the snowfall increases to a certain degree ($\sim 1 \text{ mm day}^{-1}$), it will trigger a continuous flooding process, accelerating the sea ice growth and slowing down the snow layer thickening.

Acknowledgments

The authors would like to thank ECMWF for the ERA5 reanalysis data set and the Russian meteorological station Progress II for the precipitation observations. We are grateful to CICE Consortium for sharing ICEPACK and its documentation (<https://github.com/CICE-Consortium/Icepack>). This study is supported by the National Natural Science Foundation of China (No. 41941009, 41922044), the Guangdong Basic and Applied Basic Research Foundation (No. 2020B1515020025), the Southern Marine Science and Engineering Guangdong Laboratory (Zhuhai) (No. SML2020SP007), and CAS "Light of West China" Program (No. E129030101, Y929641001). PH was supported by AAS grant 4506.

References

- Barthélemy, A., Goosse, H., Fichefet, T., and Lecomte, O.: On the sensitivity of Antarctic sea ice model biases to atmospheric forcing uncertainties, *Clim. Dynam.*, 51, 1585-1603, 2018.
- Bitz, C. M., Holland, M. M., Weaver, A. J., and Eby, M.: Simulating the ice - thickness distribution in a coupled climate model, *Journal of Geophysical Research: Oceans*, 106, 2441-2463, 2001.
- Bracegirdle, T. J., and Marshall, G. J.: The reliability of Antarctic tropospheric pressure and temperature in the latest global reanalyses, *J. Climate*, 25, 7138-7146, 2012.
- Briegleb, B. P., and Light, B.: A Delta-Eddington multiple scattering parameterization for solar radiation in the sea ice component of the Community Climate System Model, NCAR Tech. Note NCAR/TN-472+STR, 1-108, 2007.
- Bromwich, D. H., Fogt, R. L., Hodges, K. I., and Walsh, J. E.: A tropospheric assessment of the ERA - 40, NCEP, and JRA - 25 global reanalyses in the polar regions, *Journal of Geophysical Research: Atmospheres*, 112, D10111, 2007.
- Chemke, R., and Polvani, L. M.: Using multiple large ensembles to elucidate the discrepancy between the 1979 - 2019 modeled and observed Antarctic sea ice trends, *Geophys. Res. Lett.*, 47, e2020G-e88339G, 2020.
- Cheng, B., Mäkynen, M., Similä, M., Rontu, L., and Vihma, T.: Modelling snow and ice thickness in the coastal Kara Sea, Russian Arctic, *Ann. Glaciol.*, 54, 105-113, 2013.
- Cheng, B., Zhang, Z., Vihma, T., Johansson, M., Bian, L., Li, Z., and Wu, H.: Model experiments on snow and ice thermodynamics in the Arctic Ocean with CHINARE 2003 data, *Journal of Geophysical Research: Oceans*, 113, C9020, 2008.
- Collins, W. D., Bitz, C. M., Blackmon, M. L., Bonan, G. B., Bretherton, C. S., Carton, J. A., Chang, P., Doney, S. C., Hack, J. J., and Henderson, T. B.: The community climate system model version 3 (CCSM3), *J. Climate*, 19, 2122-2143, 2006.
- Fairall, C. W., Bradley, E. F., Hare, J. E., Grachev, A. A., and Edson, J. B.: Bulk parameterization of air-sea fluxes: Updates and verification for the COARE algorithm, *J. Climate*, 16, 571-591, 2003.
- Fréville, H., Brun, E., Picard, G., Tatarinova, N., Arnaud, L., Lanconelli, C., Reijmer, C., and Van den Broeke, M.: Using MODIS land surface temperatures and the Crocus snow model to understand the warm bias of ERA-Interim reanalyses at the surface in Antarctica, *The Cryosphere*, 8, 1361-1373, 2014.
- Frezzotti, M., Pourchet, M., Flora, O., Gandolfi, S., Gay, M., Urbini, S., Vincent, C., Becagli, S., Gagnani, R., and Proposito, M.: Spatial and temporal variability of snow accumulation in East Antarctica from traverse data, *J. Glaciol.*, 51, 113-124, 2005.
- Gascoin, S., Lhermitte, S., Kinnard, C., Bortels, K., and Liston, G. E.: Wind effects on snow cover in Pascua-Lama, Dry Andes of Chile, *Adv. Water Resour.*, 55, 25-39, 2013.
- Granskog, M. A., Leppäranta, M., Kawamura, T., Ehn, J., and Shirasawa, K.: Seasonal development of the properties and composition of landfast sea ice in the Gulf of Finland, the Baltic Sea, *Journal of Geophysical Research: Oceans*, 109, 10.1029/2003JC001874, 2004.
- Hao, G., Pirazzini, R., Yang, Q., Tian, Z., and Liu, C.: Spectral albedo of coastal landfast sea ice in Prydz Bay, Antarctica, *J. Glaciol.*, 67, 1-11, 2020.
- Hao, G., Yang, Q., Zhao, J., Deng, X., Yang, Y., Duan, P., Zhang, L., Li, C., and Cui, L.: Observation and analysis of landfast ice surrounding Zhongshan Station, Antarctic in 2016, *Haiyang Xuebao*, 9, 26-39, 2019.
- Heil, P.: Atmospheric conditions and fast ice at Davis, East Antarctica: A case study, *Journal of Geophysical Research: Oceans*, 111, C5009, 2006.

538 Heil, P., Allison, I., and Lytle, V. I.: Seasonal and interannual variations of the oceanic heat flux under a
 539 landfast Antarctic sea ice cover, *Journal of Geophysical Research: Oceans*, 101, 25741-25752, 1996.
 540 Hersbach, H., Bell, B., Berrisford, P., Hirahara, S., Horányi, A., Muñoz Sabater, J., Nicolas, J., Peubey,
 541 C., Radu, R., and Schepers, D.: The ERA5 global reanalysis, *Q. J. Roy. Meteor. Soc.*, 146, 1999-2049,
 542 2020.
 543 Hersbach, H., and Dee, D.: ERA5 reanalysis is in production, *ECMWF Newsletter* 147, Reading, UK:
 544 ECMWF. [Retrieved from <https://www.ecmwf.int/en/newsletter/147/news/era5-reanalysis-production>],
 545 2016.
 546 Hunke, E., Allard, R., Bailey, D. A., Blain, P., Craig, T., Dupont, F., DuVivier, A., Grumbine, R., Hebert,
 547 D., Holland, M., Jeffery, N., Lemieux, J., Rasmussen, T., Ribergaard, M., Roberts, A., Turner, M., and
 548 Winton, M.: CICE-Consortium/Icepack: Icepack1.1.1, doi:10.5281/zenodo.3251032, 2019.
 549 Jeffries, M. O., Krouse, H. R., Hurst-Cushing, B., and Maksym, T.: Snow-ice accretion and snow-cover
 550 depletion on Antarctic first-year sea-ice floes, *Ann. Glaciol.*, 33, 51-60, DOI:
 551 10.3189/172756401781818266, 2001.
 552 Jones, R. W., Renfrew, I. A., Orr, A., Webber, B., Holland, D. M., and Lazzara, M. A.: Evaluation of
 553 four global reanalysis products using in situ observations in the Amundsen Sea Embayment, Antarctica,
 554 *Journal of Geophysical Research: Atmospheres*, 121, 6240-6257, 2016.
 555 Kawamura, T., Ohshima, K. I., Takizawa, T., and Ushio, S.: Physical, structural, and isotopic
 556 characteristics and growth processes of fast sea ice in Lützow-Holm Bay, Antarctica, *Journal of*
 557 *Geophysical Research: Oceans*, 102, 3345-3355, 10.1029/96JC03206, 1997.
 558 Krumpen, T., Birrien, F., Kauker, F., Rackow, T., Albedyll, L. V., Angelopoulos, M., Belter, H. J.,
 559 Bessonov, V., Damm, E., and Dethloff, K.: The MOSAiC ice floe: sediment-laden survivor from the
 560 Siberian shelf, *The Cryosphere*, 14, 2173-2187, 2020.
 561 Lei, R., Li, Z., Cheng, B., Zhang, Z., and Heil, P.: Annual cycle of landfast sea ice in Prydz Bay, east
 562 Antarctica, *Journal of Geophysical Research: Oceans*, 115, C2006, 2010.
 563 Leppäranta, M.: A growth model for black ice, snow ice and snow thickness in subarctic basins,
 564 *Hydrology Research*, 14, 59-70, 1983.
 565 Lindsay, R., Wensnahan, M., Schweiger, A., and Zhang, J.: Evaluation of seven different atmospheric
 566 reanalysis products in the Arctic, *J. Climate*, 27, 2588-2606, 2014.
 567 Lindsay, R., and Schweiger, A.: Arctic sea ice thickness loss determined using subsurface, aircraft, and
 568 satellite observations, *The Cryosphere*, 9, 269-283, 2015.
 569 Liston, G. E., Polashenski, C., Rösel, A., Itkin, P., King, J., Merkouriadi, I., and Haapala, J.: A distributed
 570 snow - evolution model for sea - ice applications (SnowModel), *Journal of Geophysical Research:*
 571 *Oceans*, 123, 3786-3810, 2018.
 572 Liu, C., Gao, Z., Yang, Q., Han, B., Wang, H., Hao, G., Zhao, J., You, L., Yang, Y., Wang, L., Li, Y.:
 573 Observed surface fluxes over sea ice near Antarctic Zhongshan station from April to November in 2016,
 574 *Annals of Glaciology*, 61(82), 12-23, 2020.
 575 Massom, R. A., Eicken, H., Hass, C., Jeffries, M. O., Drinkwater, M. R., Sturm, M., Worby, A. P., Wu,
 576 X., Lytle, V. I., and Ushio, S.: Snow on Antarctic sea ice, *Rev. Geophys.*, 39, 413-445, 2001.
 577 Massonnet, F., Fichet, T., Goosse, H., Vancoppenolle, M., Mathiot, P., and König Beatty, C.: On the
 578 influence of model physics on simulations of Arctic and Antarctic sea ice, *The Cryosphere*, 5, 687-699,
 579 2011.
 580 Maykut, G. A., and Untersteiner, N.: Some results from a time-dependent thermodynamic model of sea
 581 ice, *Journal of Geophysical Research (1896-1977)*, 76, 1550-1575, 10.1029/JC076i006p01550, 1971.

582 McPhee, M. G., Kottmeier, C., and Morison, J. H.: Ocean Heat Flux in the Central Weddell Sea during
583 Winter, *J. Phys. Oceanogr.*, 29, 1166-1179, 10.1175/1520-0485(1999)029<1166:OHFITC>2.0.CO;2,
584 1999.

585 Merkouriadi, I., Liston, G. E., Graham, R. M., and Granskog, M. A.: Quantifying the potential for snow -
586 ice formation in the Arctic Ocean, *Geophys. Res. Lett.*, 47, e2019G-e85020G, 2020.

587 Parkinson, C. L.: A 40-y record reveals gradual Antarctic sea ice increases followed by decreases at rates
588 far exceeding the rates seen in the Arctic, *Proceedings of the National Academy of Sciences*, 116, 14414-
589 14423, 2019.

590 Parkinson, C. L., and Cavalieri, D. J.: Antarctic sea ice variability and trends, 1979-2010, *The Cryosphere*,
591 6, 871-880, 2012.

592 Perovich, D. K., and Maykut, G. A.: Solar heating of a stratified ocean in the presence of a static ice
593 cover, *Journal of Geophysical Research: Oceans*, 95, 18233-18245, 10.1029/JC095iC10p18233, 1990.

594 Provost, C., Sennéchal, N., Miguet, J., Itkin, P., Rösel, A., Koenig, Z., Villaciers Robineau, N., and
595 Granskog, M. A.: Observations of flooding and snow - ice formation in a thinner Arctic sea - ice regime
596 during the N - ICE2015 campaign: Influence of basal ice melt and storms, *Journal of Geophysical*
597 *Research: Oceans*, 122, 7115-7134, 2017.

598 Saloranta, T. M.: Modeling the evolution of snow, snow ice and ice in the Baltic Sea, *Tellus A: Dynamic*
599 *Meteorology and Oceanography*, 52, 93-108, 2000.

600 Schlosser, E., Haumann, F. A., and Raphael, M. N.: Atmospheric influences on the anomalous 2016
601 Antarctic sea ice decay, *The Cryosphere*, 12, 1103-1119, 2018.

602 Stroeve, J. C., Serreze, M. C., Holland, M. M., Kay, J. E., Malanik, J., and Barrett, A. P.: The Arctic' s
603 rapidly shrinking sea ice cover: a research synthesis, *Climatic Change*, 110, 1005-1027, 2012.

604 Stuecker, M. F., Bitz, C. M., and Armour, K. C.: Conditions leading to the unprecedented low Antarctic
605 sea ice extent during the 2016 austral spring season, *Geophys. Res. Lett.*, 44, 9008-9019, 2017.

606 Tanji, S., Inatsu, M., and Okaze, T.: Development of a snowdrift model with the lattice Boltzmann
607 method, *Progress in Earth and Planetary Science*, 8, 1-16, 2021.

608 Tetzner, D., Thomas, E., and Allen, C.: A Validation of ERA5 Reanalysis Data in the Southern Antarctic
609 Peninsula—Ellsworth Land Region, and Its Implications for Ice Core Studies, *Geosciences*, 9, 289, 2019.

610 Thiery, W., Gorodetskaya, I. V., Bintanja, R., Van Lipzig, N., Van den Broeke, M. R., Reijmer, C. H.,
611 and Kuipers Munneke, P.: Surface and snowdrift sublimation at Princess Elisabeth station, East
612 Antarctica, *The Cryosphere*, 6, 841-857, 2012.

613 Turner, A. K., Hunke, E. C., and Bitz, C. M.: Two modes of sea-ice gravity drainage: A parameterization
614 for large - scale modeling, *Journal of Geophysical Research: Oceans*, 118, 2279-2294, 2013.

615 Turner, A. K., and Hunke, E. C.: Impacts of a mushy-layer thermodynamic approach in global sea-ice
616 simulations using the CICE sea-ice model, *Journal of Geophysical Research: Oceans*, 120, 1253-1275,
617 2015.

618 Turner, J., Phillips, T., Marshall, G. J., Hosking, J. S., Pope, J. O., Bracegirdle, T. J., and Deb, P.:
619 Unprecedented springtime retreat of Antarctic sea ice in 2016, *Geophys. Res. Lett.*, 44, 6868-6875,
620 2017. Uotila, P., Goosse, H., Haines, K., Chevallier, M., Barthélemy, A., Bricaud, C., Carton, J., Fučkar,
621 N., Garric, G., and Iovino, D.: An assessment of ten ocean reanalyses in the polar regions, *Clim. Dynam.*,
622 52, 1613-1650, 2019.

623 Urraca, R., Huld, T., Gracia-Amillo, A., Martinez-de-Pison, F. J., Kaspar, F., and Sanz-Garcia, A.:
624 Evaluation of global horizontal irradiance estimates from ERA5 and COSMO-REA6 reanalyses using
625 ground and satellite-based data, *Sol. Energy*, 164, 339-354, 2018.

626 Van Den Broeke, M. R., Winther, J., Isaksson, E., Pinglot, J. F., Karlöf, L., Eiken, T., and Conrads, L.:
 627 Climate variables along a traverse line in Dronning Maud Land, East Antarctica, *J. Glaciol.*, 45, 295-302,
 628 1999.
 629 Van den Broeke, M. R., Reijmer, C. H., and Van De Wal, R. S.: A study of the surface mass balance in
 630 Dronning Maud Land, Antarctica, using automatic weather stations, *J. Glaciol.*, 50, 565-582, 2004.
 631 Vancoppenolle, M., Timmermann, R., Ackley, S. F., Fichefet, T., Goosse, H., Heil, P., Leonard, K. C.,
 632 Lieser, J., Nicolaus, M., and Papakyriakou, T.: Assessment of radiation forcing data sets for large-scale
 633 sea ice models in the Southern Ocean, *Deep Sea Research Part II: Topical Studies in Oceanography*, 58,
 634 1237-1249, 2011.
 635 Vignon, É., Traullé, O., and Berne, A.: On the fine vertical structure of the low troposphere over the
 636 coastal margins of East Antarctica, *Atmos. Chem. Phys.*, 19, 4659-4683, 2019.
 637 Wang, C., Graham, R. M., Wang, K., Gerland, S., and Granskog, M. A.: Comparison of ERA5 and ERA-
 638 Interim near-surface air temperature, snowfall and precipitation over Arctic sea ice: effects on sea ice
 639 thermodynamics and evolution, *The Cryosphere*, 13, 1661-1679, 2019b.
 640 Wang, G., Hendon, H. H., Arblaster, J. M., Lim, E., Abhik, S., and van Rensch, P.: Compounding tropical
 641 and stratospheric forcing of the record low Antarctic sea-ice in 2016, *Nat. Commun.*, 10, 1-9, 2019a.
 642 Wang, Y., Zhou, D., Bunde, A., and Havlin, S.: Testing reanalysis data sets in Antarctica: Trends,
 643 persistence properties, and trend significance, *Journal of Geophysical Research: Atmospheres*, 121, 12-
 644 839, 2016.
 645 Yang, Q., Liu, J., Leppäranta, M., Sun, Q., Li, R., Zhang, L., Jung, T., Lei, R., Zhang, Z., and Li, M.:
 646 Albedo of coastal landfast sea ice in Prydz Bay, Antarctica: Observations and parameterization, *Adv.*
 647 *Atmos. Sci.*, 33, 535-543, 2016a.
 648 Yang, Y., Zhijun, L., Leppäranta, M., Cheng, B., Shi, L., and Lei, R.: Modelling the thickness of landfast
 649 sea ice in Prydz Bay, East Antarctica, *Antarct. Sci.*, 28, 59-70, 2016b.
 650 Zhang, J.: Increasing Antarctic sea ice under warming atmospheric and oceanic conditions, *J. Climate*,
 651 20, 2515-2529, 2007.
 652 Zhang, J.: Modeling the impact of wind intensification on Antarctic sea ice volume, *J. Climate*, 27, 202-
 653 214, 2014.
 654 Zhao, J., Cheng, B., Yang, Q., Vihma, T., and Zhang, L.: Observations and modelling of first-year ice
 655 growth and simultaneous second-year ice ablation in the Prydz Bay, East Antarctica, *Ann. Glaciol.*, 58,
 656 59-67, 2017.
 657 Zhao, J., Cheng, B., Vihma, T., Yang, Q., Hui, F., Zhao, B., Hao, G., Shen, H., and Zhang, L.:
 658 Observation and thermodynamic modeling of the influence of snow cover on landfast sea ice thickness
 659 in Prydz Bay, East Antarctica, *Cold Reg. Sci. Technol.*, 168, 102869, 2019.
 660